Freezing, melting, nonwetting, and coexistence in (KCl)$_{32}$

John P. Rose and R. Stephen Berry
Department of Chemistry and The James Franck Institute, The University of Chicago, Chicago, Illinois 60637

Binary clusters, notably salt clusters with their combination of attractive and repulsive long-range forces, exhibit structural and dynamical behavior different from that of homogeneous clusters. The melting and freezing, nonwetting, and the complexity of the potential surface of (KCl)$_{32}$ are used to make the comparison. A new method to estimate the density of configurational states is described and applied to the evaluation of thermodynamic properties of (KCl)$_{32}$. In particular, with this new method we compute for several temperatures the fraction or probability, $P(\phi,\beta)$, of clusters vibrating around a configuration with minimum energy ϕ. The behavior of $P(\phi,\beta)$ with temperature T is indicative of a coexistence of solidlike and liquidlike forms of (KCl)$_{32}$ for a range of temperatures. The input data required by this new method can be obtained from constant temperature molecular dynamics simulations.

I. INTRODUCTION

Theoretical work on clusters has concentrated heavily on homogeneous clusters of spherically symmetric species modeled by simple Lennard-Jones[1-7] or Morse[8] potentials. On the basis of these studies a theoretical framework has been developed[9-13] that explains and predicts well the behavior of clusters. In its early stages, the generality of this maturing framework was restricted by the lack of diversity of clusters studied. However, the list of different clusters studied has grown long and varied; heterogeneous clusters (alkali halides,[14-25] rare gases doped with a large organic molecule,[26,27] and rare gases doped with alkali halides[28]), alkali[29] and transition metals,[30-34] molecular van der Waals clusters,[35-38] and nonmetal[39] clusters. (For an extensive collection of papers on a variety of cluster topics see Refs. 40 and 41). In spite of this impressive list there still is much to be learned about the variability of cluster behavior. In particular, little is known from experiments about the phase coexistence behavior of clusters. Experiments germane to much of the theoretical work, on pure, size-selected rare gas clusters, would be extremely difficult. However, relevant experiments on clusters that are more tractable both experimentally and for theory, such as alkali halides, may be possible.

Alkali halide clusters are good model systems because they are amenable to both theory and experiment. On the theory side, a realistic, pairwise additive potential describes them well. Studies have shown that more exact alkali halide potentials give essentially the same statics as does the simple Born–Mayer potential.[15,25,42] Work on alkali halide clusters by Martin[16-20] and Welch *et al.*[14,15] focused on the geometries and vibrational properties of small and intermediate-size clusters. Luo, Landman, and Jortner[21] investigated the dynamics of three NaCl clusters, (NaCl)$_4$, (NaCl)$_{16}$, and (NaCl)$_{108}$. They found that the behavior of NaCl clusters depends strongly on the size of the cluster; small NaCl clusters exhibit simple isomerization dynamics, large NaCl clusters exhibit freezing/melting behavior similar to rare gas clusters and intermediate size NaCl clusters exhibit dynamics that are a combination of the small and large size limiting cases. The isomerization kinetics of (NaCl)$_4$ have been studied in further detail by Heidenreich and co-workers.[22,23]

Recently, we presented a fairly comprehensive investigation of small KCl clusters, namely, (KCl)$_4$ and (KCl)$_5$.[24] In this study the cluster dynamics were explained by relating them to the features of the underlying multidimensional potential energy surface. To complement and compare this study of small KCl clusters we undertook the study of (KCl)$_{32}$, which we chose for a few specific reasons. First, (KCl)$_{32}$ has a simple symmetric $4\times4\times4$ ground state structure, making it easy to locate. Second, if we consider the symmetric $2n\times2n\times2n$ KCl clusters to be alkali halide magic number clusters then (KCl)$_{32}$ is the second smallest magic number cluster and we can compare it to the smallest magic number cluster (KCl)$_4$. Magic number clusters are important experimentally because their conspicuous stability, compared to their nearby size neighbors, may mean they can be prepared in high enough abundance to facilitate experiments. Lastly, (KCl)$_{32}$ is large enough to have distinct surface and interior particles but at the same time it is not too large to make potential energy minimizations computationally difficult. (Many potential energy minimizations must be done in order to map a potential surface, so they must be cheap and relatively quick to complete.)

In the next section we briefly explain the methods used in this study. In Sec. III we present and discuss our results, dividing them into three subsections: (A) phase behavior, (B) nonwetting behavior, and (C) density of configurational states. In Sec. III C we describe a new method to estimate the density of configurational states and compare it with simulation results. Lastly, in Sec. IV we make a few concluding statements regarding the interpretation of the results.

II. METHODS

(KCl)$_{32}$ was studied by a combination of four techniques: constant energy and constant temperature molecular dynamics (MD), potential energy surface minimizations, and analytic statistical mechanical theory. The intention of the analytic theory was to derive and apply an expression for the density of configurational states which could be evaluated using simulation data as the input. The MD method is well known and has been explained many times elsewhere,[43–45] so we will only discuss the main points particular to our study.

The velocity form of the Verlet propagation algorithm[44] was used to integrate the constant energy MD equations of motion. A time step of 3×10^{-15} was required to conserve the energy from step to step to at least five significant digits and also to prevent the energy from drifting over time. Constant energy trajectories of 10^5 times steps, preceded by an equilibrium period of 10^3 time steps, were run to calculate quantities such as the average vibrational temperature, relative root-mean-square bond length fluctuation δ, mean square displacement (MSD), and the velocity autocorrelation function. For a thorough explanation of these quantities see Ref. 24.

The Nosé equations of motion[46,47] were used for the constant temperature MD. The forces in the Nosé method are velocity dependent, so it is necessary to use a propagation algorithm that calculates accurately both the configurations and the velocities; a sixth-order Gear predictor-corrector propagator[43,48] with a time step of 3×10^{-15} was used to accomplish this. For this study dynamical quantities were calculated only with constant energy MD. Previous work on Ar$_{13}$ compared dynamical quantities calculated with constant temperature simulations, both Monte Carlo and MD, with constant energy MD results and found enough agreement to infer that the conclusions were not dependent on the ensemble.[49]

Potential surface minima were located with the steepest-descent[50,51] (SD) and the conjugate gradient[52] (CG) minimization technique. In the SD method one momentarily stops the MD, effectively sets the kinetic energy to zero, and then immediately solves the differential equation

$$\frac{dr}{dt} = -\nabla \Phi(r) \qquad (1)$$

until a potential minimum is found. In the CG method, at each incremental step the potential energy of the system is minimized along $3N-6$ mutually conjugate, "noninterfering" directions. Noninterfering means that the minimizations performed along each of these conjugate directions are independent of all the others. That is, the minimization along one direction does not spoil the minimizations along all the other conjugate directions.[52] The minimization process (either SD or CG) is entirely independent of the MD. The MD trajectory is not altered by the minimization process; it merely provides a distribution of starting configurations for the chosen quench process. For a discussion of

the mathematics and necessary FORTRAN code for the CG method, see Ref. 52.

To locate the minima of the (KCl)$_{32}$ potential surface the CG method was used almost exclusively because it proved to be more efficient than the SD method. Nevertheless, the SD method was applied to quenched geometries reached by CG, and also both minimization techniques were applied to some of the same starting geometries, to check the accuracy or at least the consistency of the CG method. Occasionally from the same high-energy starting geometries the SD and CG methods located different minima. Such behavior is not surprising for a highly convoluted surface. This presents no problems; rather, for a surface with a large number of minima, finding the individual minima is less important than obtaining a large statistical sample of minima, including some that are close in configuration space. This is an important point that distinguishes the coarse-grained approach one must adopt when studying a large cluster such as (KCl)$_{32}$ from the fully detailed view we can use with small clusters such as (KCl)$_4$ or (KCl)$_5$.

The Born–Mayer[53,54] type potential used for this study is the same one that we used previously[24] to study (KCl)$_4$ and (KCl)$_5$ and was also used for many other computer simulation studies of alkali halides,[14–23]

$$\Phi = \sum_{i<j} \Phi_{ij} = \sum_{i<j} \left[\frac{q_i q_j}{r_{ij}} + A_{ij} \exp(-r_{ij}/\rho) \right]; \qquad (2)$$

q_i and q_j are the charges on the ions i and j, and r_{ij} is the distance between ions i and j. The first term is a Coulomb interaction and the second repulsive term approximates the effects of the Pauli exclusion forces[55] on the filled electronic shells of the ions, as they unshield the nuclear repulsions. The values of the constants A_{ij} ($A_{++} = 1555.21$ eV, $A_{+-} = 1786.91$ eV, $A_{--} = 1924.80$ eV) and ρ (0.337 Å) are those given by Tosi and Fumi.[53] The value of A_{ij} depends upon the particular interacting ions whereas ρ does not and ρ and A_{ij} are assumed to be independent of the number of particles in the cluster. Other, more elaborate model potentials for alkali halide clusters have been proposed and successfully employed in simulation studies. For example, multipole or dispersion terms can be appended to the rigid shell model potential to account for ion polarization effects.[15] For the objectives of this study, the simple rigid shell potential was entirely adequate when judged against the added complexities and increased computation time incurred by using a more exact potential. Including polarization terms in the potential would require solving a set of linear equations at each time step of the simulation in order to calculate the instantaneous dipole moments of the ions.

III. RESULTS

A. Freezing and melting of (KCl)$_{32}$

The phase behavior of many different clusters has been extensively discussed[1,9,13,24] so only a brief review will be given here. It is well established theoretically and experimentally[35,38] that some clusters can exhibit distinguishable solidlike and liquidlike states. A cluster passes between

solidlike and liquidlike forms in a manner that is the small-system analogue of the freezing/melting transition of bulk matter. We emphasize the distinction between a "phase change" of a cluster and a phase transition of bulk matter. In bulk matter the freezing/melting transition occurs sharply at a single temperature for each pressure, whereas the ratio of liquidlike to solidlike forms of an ensemble of a given kind and size of clusters changes gradually within a finite band of temperatures. In some clusters this effect manifests itself as unequal limiting temperatures for freezing and melting, T_f and T_m, respectively, where T_f is the lower temperature limit for the stability of the liquidlike cluster and T_m is the upper temperature limit of stability for the solidlike cluster. Although there is theoretical evidence[56,57] that these limits of stability can be extrapolated to the bulk, the macroscopic number of particles conceals this from observation, both experimentally and in simulations. In this respect, the observable details of the phase behavior of clusters differs from that of the bulk.

Our approach here, as done previously,[10,13,24] is to rationalize the thermodynamics and dynamics of (KCl)$_{32}$ by relating the simulation results to the structure of the underlying potential energy surface. The structure of a surface is mapped by determining both the geometry and topology of the surface. Geometry refers to the minima and saddle point energies and topology refers to the connectivity of the surface, i.e., which saddles connect which minima. In previous studies on small clusters, and some as large as Ar$_{55}$,[7,58] the objective was to map the potential surface in as fine detail as possible. However, for large clusters, like (KCl)$_{32}$, it is neither feasible nor sensible to describe the potential surface in meticulous detail. Besides the global minimum, only a gross understanding of the surface is necessary. An adequate coarse-grained understanding constitutes enough information to calculate average properties. It is not necessary to find all (or most) of the minima and saddles on the potential surface as we did for (KCl)$_4$ and (KCl)$_5$.

The ground state configuration of (KCl)$_{32}$ shown in Fig. 1(a) has a cubic rocksalt structure identical to the bulk potassium chloride crystal and the minimum energy of the ground state configuration, $\phi = -3.3703$ eV/ion, is 96% of the bulk crystal[15] binding energy. In this paper ϕ will represent the quenched energy of a stable structure. The next higher minimum above the ground state that we found was at $\phi = -3.3534$ eV/ion, creating an energy gap Δ of approximately 0.017 eV/ion. We say approximately because with such a complicated surface it is impossible to be absolutely certain that one has found a specific minimum, such as the lowest excited state configuration. Nevertheless, with the numerous anneals and quenches that we performed we can be highly confident that the lowest excited state that we found is at least very close to the actual one. This structure, which is shown in Fig. 1(b), is relatively quite stable because it attains the stable $3 \times 4 \times 5$ rocksalt structure with the four remaining ions situated in a line parallel to an edge of the rectangle. From this structure we can see that it is unlikely that this configuration is directly connected to the ground state by a single rank-one saddle. This is quite unlike the rare gas clusters,[1,7,58] and even bulk[59] rare gases, for which the lowest excited state is reached directly from the ground state by the creation of a simple point or surface defect. It is of course very possible that a low minimum directly connected to the rocksalt minimum might exist for (KCl)$_{32}$ but we did not find any. In fact, we checked this by systematically creating singly defected crystalline structures. This was accomplished by manually removing an ion from a corner of the perfect rocksalt microcrystal, placing it on a face or edge, and then subsequently quenching the fabricated structure. Placing the defect ion on a face produced a structure with energy of $\phi = -3.3379$ eV/ion and on an edge $\phi = -3.3391$ eV/ion. Some of the other minima that are directly connected to the ground state were identified by simulations, but they also all had energies greater than -3.3534 eV/ion.

Above the energy gap Δ the spectrum of locally stable structures is essentially a continuous function of energy, because the surface has so many minima. The best method we found to describe the spectrum of local minima is to separate the stable minima into four ranges. The lowest range consists of just the microcrystal ground state. The next range of energies is associated with minima corresponding to structures that are mostly regular and rocksaltlike except for a few defects; we term these structures crystal-like to distinguish them from the perfect microcrystal. The third energy range includes what we call nonwetted structures; the structures in this range are partly regular, rocksaltlike and partly highly disordered. We will say more about nonwetted structures below. The highest energy range contains a very large collection of minima that have completely disordered (amorphous) equilibrium configurations. There is no sharp physical separation, except for the energy gap Δ, that delineates these energy ranges. As a result, any choice of energy limits for these ranges is arbitrary and so we will not attempt to define them strictly. Representative structures we found for each of these four energy ranges are shown in Fig. 1. The radial distribution functions for each of the particular structures shown in Fig. 1 are shown in Fig. 2.

We chose to define these energy ranges in this way because there is a correlation between the energy of an inherent structure and its extent of order. This is shown graphically in Fig. 3. We can explain this graph best by describing how it was constructed. A collection of quenched structures, about 100, was accumulated and each one was visually classified based on its apparent extent of crystallinity. We viewed each structure on the computer; if the structure was devoid of order it was classified into the amorphous category, if it was very ordered then it was put in the category containing crystal-like structures, and if it was only partially ordered, which usually meant that at least one side or end of the cluster was rocksaltlike, we classified it as nonwetted. This was all done without prior knowledge of the energy of the structures. After each structure was classified it was paired with its energy. Lastly, a histogram plot was generated from the energies in each category except for the microcrystal category. Notice in Fig. 3 the clear separation between the distribution of
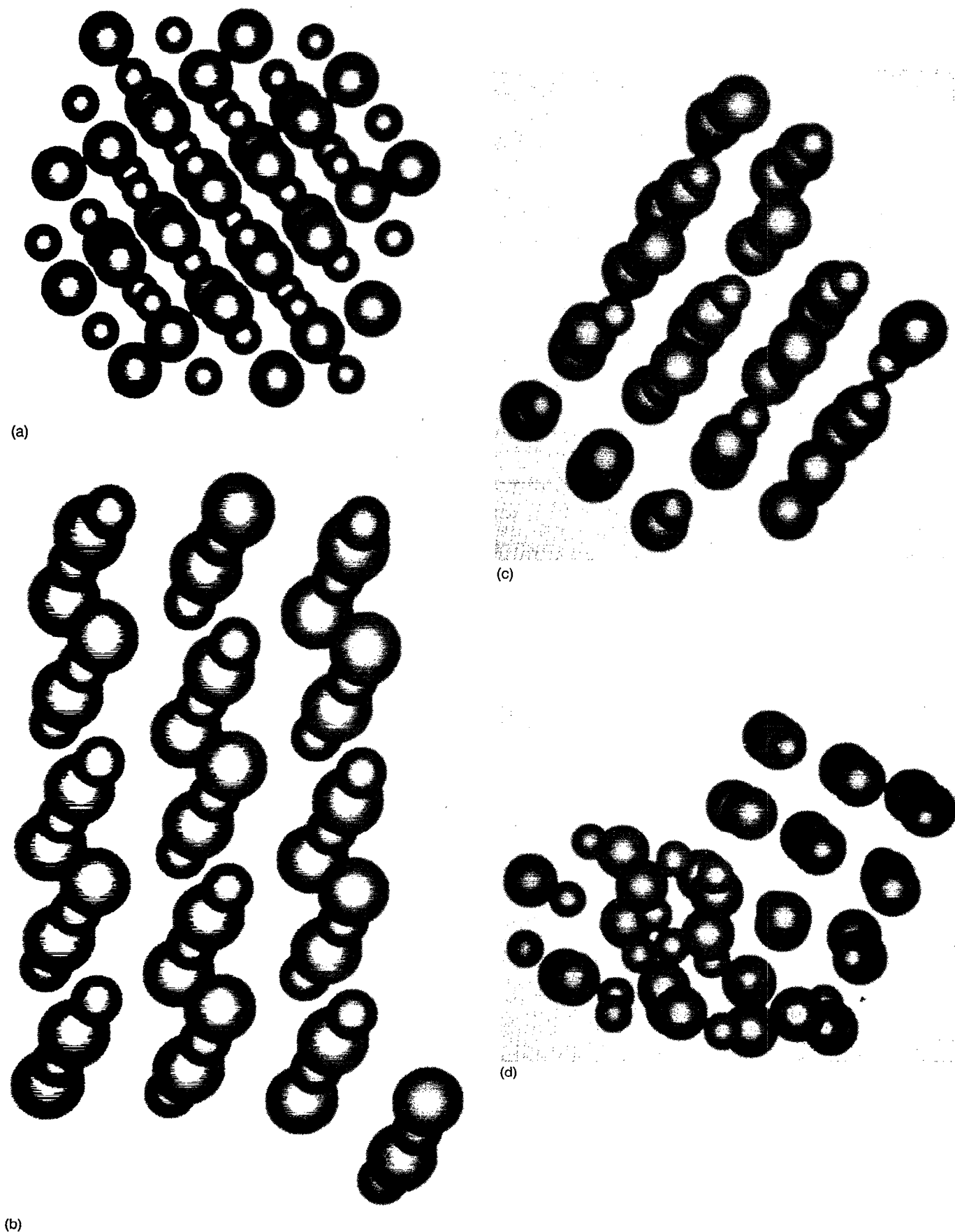
FIG. 1. Five representative structures for (KCl)$_{32}$; (a) microcrystal, $\phi = -3.3703$ eV/ion, (b) lowest excited state configuration, $\phi = -3.3534$ eV/ion, (c) crystal-like structure, $\phi = -3.3465$ eV/ion, (d) nonwetted structure, $\phi = -3.3254$ eV/ion (e) amorphous structure, $\phi = -3.2993$ eV/ion.
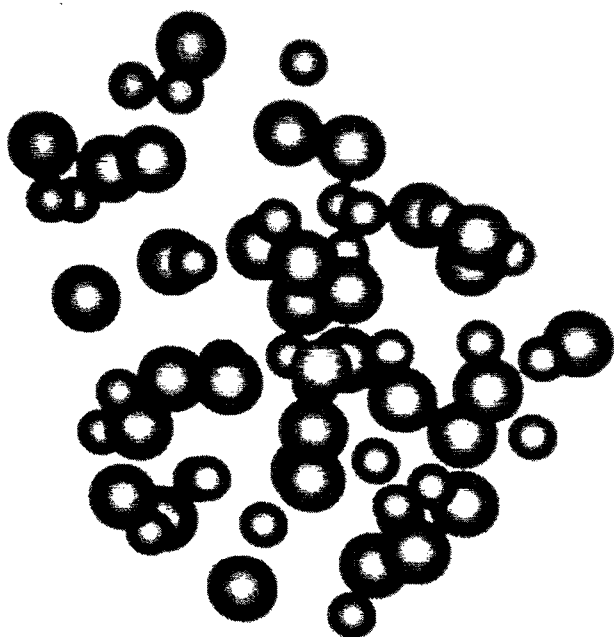
FIG. 1. (Continued.)

quenched energies for the amorphous and crystal-like categories. As anticipated the distribution of minima energies for nonwetted structures falls into a range intermediate between the crystal-like and amorphous ranges, and not surprisingly overlaps both of them.

The caloric curves derived by MD for (KCl)$_{32}$ are shown in Fig. 4. The kinetic temperature of a cluster at constant energy is defined by the equipartition theorem for a system with $3N$-6 vibrational degrees of freedom. For the constant temperature caloric curve the mean total energy E of the caloric curve is obtained as an average over a constant temperature trajectory.[46,47] The flat region around 750 K in both caloric curves marks the onset of melting in (KCl)$_{32}$. The flat region is a manifestation of the sudden change in the regions of the potential surface that the cluster explores.[9,11,13,24] At low energies (temperatures) below the onset of melting, or of any kind of rearrangements, the cluster vibrates only around the most stable isomer. At some higher energy the cluster explores regions of the surface unexplored at lower energies. If the new regions differ significantly in potential energy from the lowest energy region, and if there is a time scale separation between interwell and intrawell motions, then this potential energy difference is revealed by a flat region or loop feature in the caloric curve.[4,11] Note, when we refer to a temperature we mean either the temperature of a constant temperature trajectory or the long-time average kinetic temperature of a constant energy trajectory.

A multidimensional potential energy surface can be partitioned into distinct contiguous regions. Each region is the catchment basin for a single potential minimum (or in rare cases, a saddle). The geometric structure of a potential minimum is called the inherent structure of that basin.[50,51] At any temperature T each basin has an occupation prob-

ability whose logarithm is the entropy associated with that basin. At a less prescribed level, at temperature T, the set of basins with minimum energy $\phi \pm \delta\phi$ has an occupation probability and a corresponding entropy. We express this probability distribution function as $P(\phi,T)$, where ϕ is the minimum energy of a catchment basin. Thus $P(\phi,T)$ is the normalized probability density, at T, of finding the cluster vibrating within any basin with minimum energy ϕ. Small clusters with a discrete number of permutationally nonequivalent basins, have a discrete $P(\phi,T)$ that, for most T must be represented by the complete set of occupation probabilities, a particular probability for each basin. Bulk systems with an enormous number of basins, on the order of e^N for a system of N particles, have a continuous $P(\phi,T)$, which we conjecture is a sharply peaked function of ϕ for each fixed T. If $P(\phi,T)$ is sharply and uniquely peaked then the entire distribution can be represented by a single number ϕ_m, the energy associated with the peak probability. The more closely $P(\phi,T)$ resembles a delta function the more powerful is this representation. Because the energy ϕ_m of the peak probability depends on the temperature, we write it as $\phi_m(T)$. With respect to the shape of the caloric curve the crucial issue is how $P(\phi,T)$ changes with T.

When in its solidlike form (KCl)$_{32}$ vibrates within the global minimum basin, thus $\phi_m = \phi_{\text{crystal}} = -3.3703$ eV/ion. At the onset of melting (KCl)$_{32}$ begins to access the basins of its locally stable isomers. However, from simulations we found that the cool liquid does not spend much time around its low-lying local minima, but instead in basins with $\phi \approx -3.313$ eV/ion. Thus when (KCl)$_{32}$ melts its $P(\phi,T)$ function changes from just a delta function centered on the energy of the global minimum to a distribution that has significant probability for $\phi = -3.313$ eV/ion. When (KCl)$_{32}$ passes out of its global minimum potential basin it occupies the high-energy local minima instead of the very low-energy local minima because there are so many more high-energy minima than there are low-energy local minima; entropy wins out over energy. This fairly sharp change in $P(\phi,T)$ is the source of the flat region in the caloric curve. Although this change is fairly sharp, it nonetheless must still be continuous as evidenced by the rounding of the transition region of the caloric curve [Fig. 4(a)]. A rounded transition region in the caloric curve is suggestive of a solidlike/liquidlike phase coexistence.[60] We discuss this topic more below.

A microscopic quantity used to locate the melting point for a cluster is the relative root-mean-square (rms) bond length fluctuation (δ) curve. The rms bond length fluctuation curve as a function of energy $\delta(E)$, or as a function of temperature $\delta(T)$, is essentially the standard deviation of the interparticle distances in units of the mean bond length, averaged over a MD trajectory. The Lindemann criterion[61,62] states that melting sets in when $\delta \approx 0.1$; δ is a sensitive function of cluster rearrangements, so a sharp increase in δ signals the onset of rearrangements responsible for melting and liquidlike behavior. The $\delta(E)$ and $\delta(T)$ curves are shown in Fig. 5. At low temperatures (energies) δ is small because the cluster lingers in the

(a)

(b)

(c)

(d)

(e)
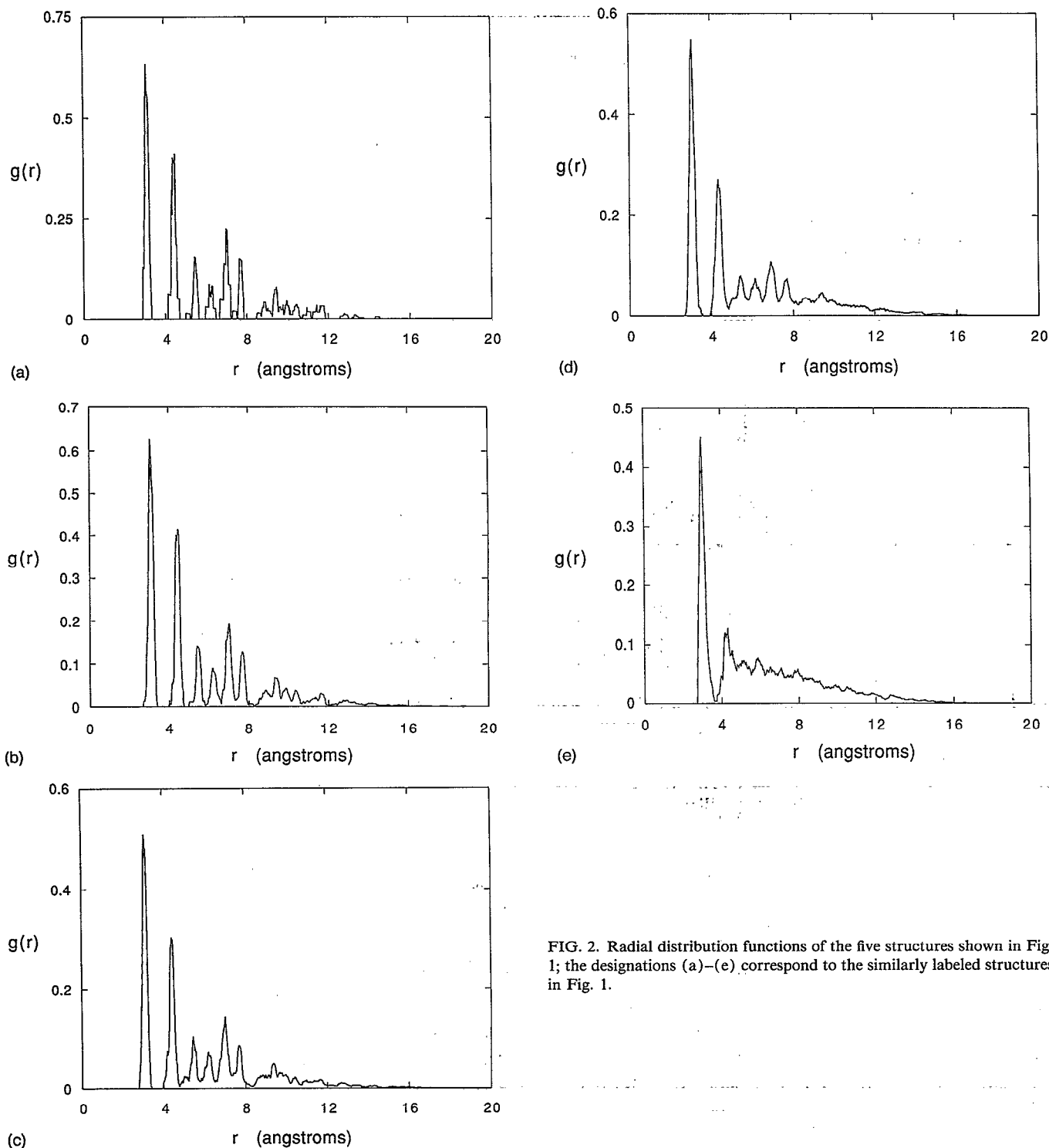
FIG. 2. Radial distribution functions of the five structures shown in Fig. 1; the designations (a)–(e) correspond to the similarly labeled structures in Fig. 1.

ground state and only undergoes solidlike, vibrational motions. At high temperatures (energies) above the sharp increase in δ, (KCl)$_{32}$ passes rapidly among a huge number of minima and is liquidlike.

Quantities such as the caloric curve, $\delta(T)$ or $\delta(E)$ are useful for locating the onset of melting of a cluster. Dynamical quantities such as the mean square displacement (MSD), $\langle r^2(t) \rangle$, or the power spectrum $I(\omega)$ are useful for establishing the state of a cluster for a given temperature and sample trajectory segment. The slope of $\langle r^2(t) \rangle$ is proportional to the diffusion constant. At a temperature

below the sharp increase in δ the MSD curve shown in Fig. 6 has nearly zero slope, which is evidence that the cluster is solidlike. The power spectrum, the Fourier transform of the velocity autocorrelation function, shown in Fig. 7(a), similarly demonstrates that the cluster is solidlike at low energies. The power spectrum in Fig. 7(a), although diffuse and broad in general shape, has negligible intensity at low frequencies, near $\omega = 0$, and pronounced peak structure at higher frequencies. The negligible low frequency intensity means that soft, diffusive, liquidlike modes are absent. The pronounced peak structure means that the
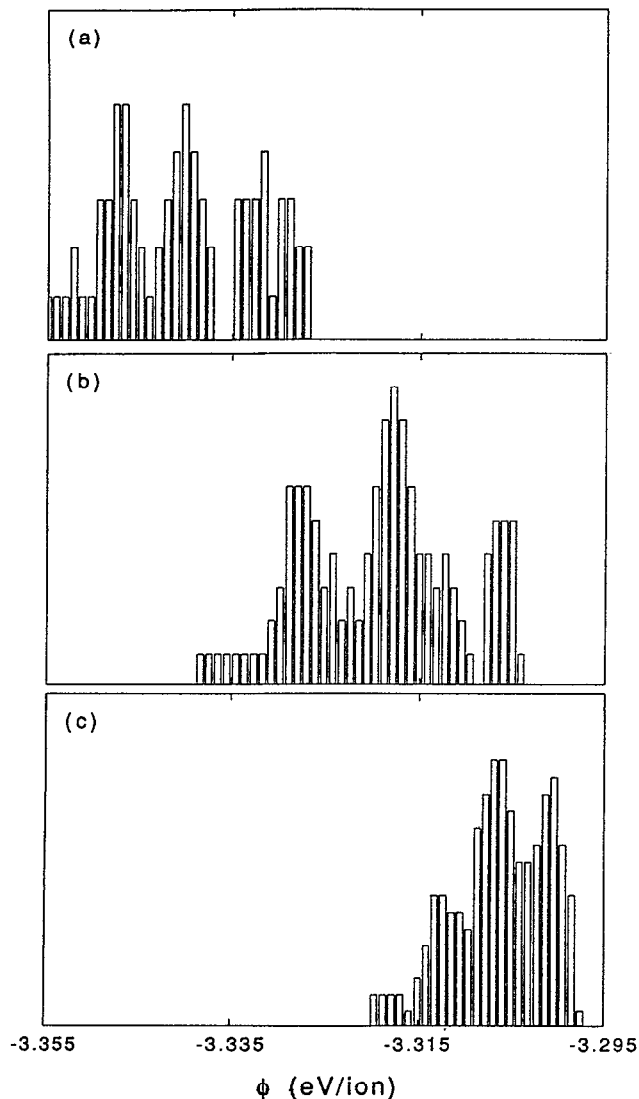
FIG. 3. Histograms of the distribution of quenched energies for the different categories of locally stable structures described in the text: (a) crystal-like structures, (b) nonwetted structures, and (c) amorphous structures.

FIG. 4. (a) Constant energy caloric curve; the open circles are the results of one caloric curve heating cycle and the filled circles are the average of six separate cycles, (b) constant temperature caloric curve; the open circles are the results of one caloric curve heating cycle and the filled circles are the average of five separate cycles. "One caloric curve heating cycle" means that the final coordinates and velocities of the MD trajectory at each energy (temperature) were the initial conditions for the MD trajectory at each successively higher energy (temperature).

cluster is undergoing some harmonic cold-molecule-type motions. Both of these qualities of $I(\omega)$ are cogent demonstration that the cold cluster is solidlike.

The onset of melting means that the total energy is high enough above the ground state energy barriers for (KCl)$_{32}$ to find a path out of its global minimum, and explore many high-lying potential wells, in the time of an average MD trajectory. The slope of the MSD (Fig. 6) at an energy above the sharp increase in $\delta(E)$, $E=-3.05$ eV/ion, is nonzero and large indicating the presence of diffusive, liquidlike motions. From the slope of the MSD at $E=-3.05$ eV/ion we can calculate the self-diffusion coefficient D of liquidlike (KCl)$_{32}$. The self-diffusion coefficient of (KCl)$_{32}$ at $E=-3.05$ eV/ion is actually larger *than the* self-diffusion constant in bulk[63] molten KCl well above the bulk melting temperature (see Table I). The

power spectrum [Fig. 7(b)] at $E=-3.05$ eV/ion is very broad, diffuse, and displays a large intensity at $\omega=0$, which also points out that there is considerable diffusive, liquidlike motion occurring.

The liquidlike phase of (KCl)$_{32}$, the second KCl magic number cluster, is significantly different from the liquidlike state of the first KCl magic number cluster, (KCl)$_4$. The interwell motions of (KCl)$_4$ are highly collective in character and therefore particle interchanges in (KCl)$_4$ occur only through a multistep rearrangement process.[24] This restricts the rate of diffusion and makes the liquidlike state of (KCl)$_4$ appear stiff compared to the liquidlike state of rare gas clusters. In comparison, the liquidlike state of (KCl)$_{32}$ is more fluidlike and less stiff, with interwell motions that are less collective than those for (KCl)$_4$. We inferred this from the large self-diffusion constant for (KCl)$_{32}$, the broad diffuse shape of the power spectrum,
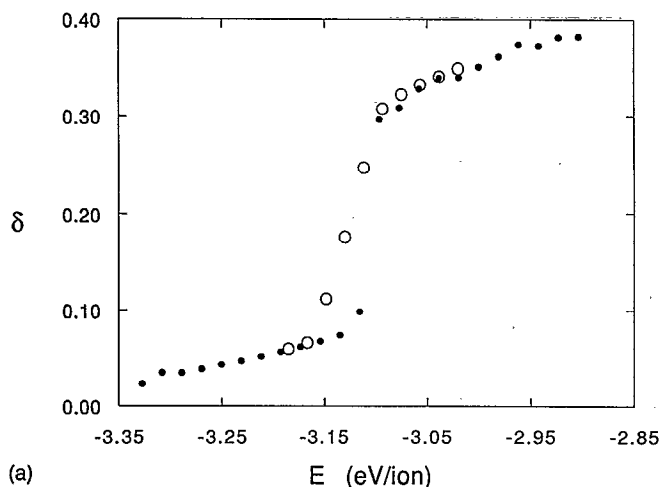
(a)
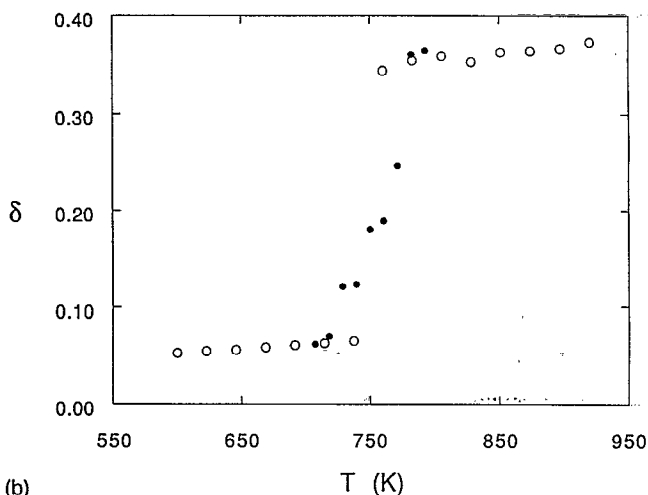
(b)

FIG. 5. (a) Constant energy root-mean-square bond length fluctuation curve $\delta(E)$; the open circles are the results of one root-mean-square bond length fluctuation curve heating cycle and the filled circles are the average of six separate cycles, (b) constant temperature root-mean-square bond length fluctuation curve $\delta(T)$; the open circles are the results of one root-mean-square bond length fluctuation curve heating cycle and the filled circles are the average of five separate cycles. "One root-mean-square bond length fluctuations curve heating cycle" means that the final coordinates and velocities of the MD trajectory at each energy (temperature) were the initial conditions for the MD trajectory at each successively higher energy (temperature).

and also from looking at MD movies on the computer. In a few tens of time steps the liquidlike dynamics of (KCl)$_{32}$ carry it from one inherent structure to another, considerably different structure.

The transition between the solidlike and liquidlike phases of (KCl)$_{32}$ is sharp in the sense that, during a particular MD trajectory, if the cluster transforms from its solidlike phase to its liquidlike phase it rarely, if ever, changes back into its solidlike phase. Extensive constant energy and temperature simulations revealed only a single case (constant T MD) in which (KCl)$_{32}$ changed from its high-potential energy, liquidlike form back into its low-potential energy, solidlike form. In this instance, the return stay in the solidlike form was relatively short and moreover, once (KCl)$_{32}$ eventually transformed back into its liquidlike form it remained liquidlike for the duration of
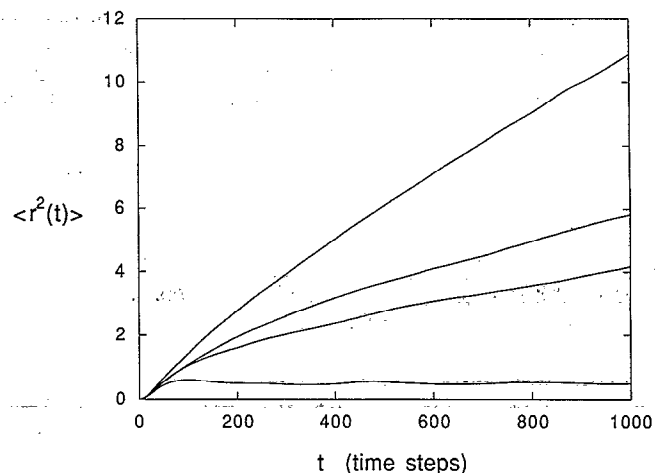
FIG. 6. Mean square displacement for (KCl)$_{32}$ at four energies; labeling from bottom to top, $E=-3.20$ eV/ion (solidlike), $E=-3.115$ eV/ion (melting region), $E=-3.107$ eV/ion (cold liquidlike) and $E=-3.05$ eV/ion (liquidlike).
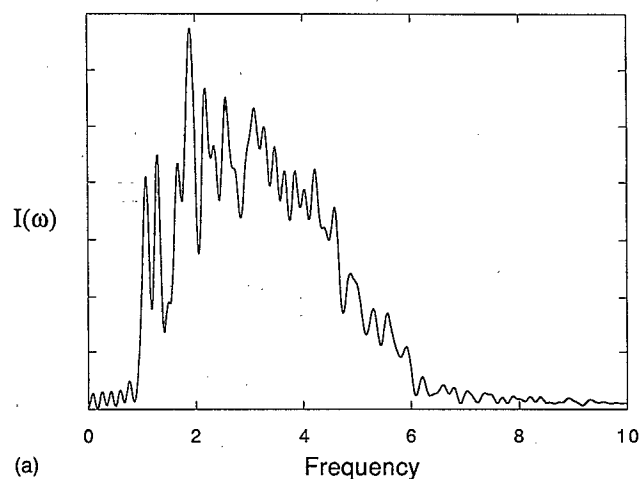
(a)
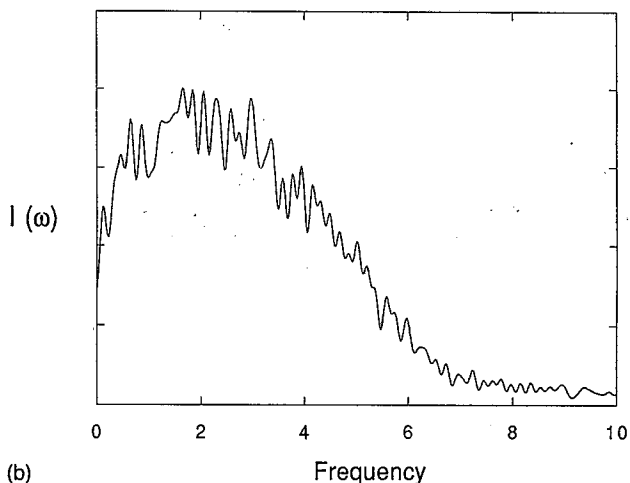
(b)

FIG. 7. Power spectra (a) $E=-3.275$ eV/ion (solidlike) and (b) $E=-3.05$ eV/ion (liquidlike). The units on the vertical scale are arbitrary and the frequency units on the horizontal scale are 10^{12} s^{-1}.

TABLE I. Representative self-diffusion constants D. The numbers for bulk KCl were calculated using Eq. (1) in Ref. 63 and the values for (KCl)$_4$ were taken from Ref. 24.

	Temperature (K)	D (10^5 cm^2/s)	Melting temperature (K)
Bulk KCl	1193	9.4[a]	1049
(KCl)$_{32}$	894	13.9	~750
(KCl)$_4$	1109	0.61	~700

[a]Average of the individual cation and anion self-diffusion constants.

the simulation ($\approx 1.5 \times 10^6$ time steps). Consistent with these findings is the sharp increase in δ [Figs. 5(a) and 5(b)], as calculated from a single MD cycle. In these curves δ jumps sharply from its low value for the solid branch up to its high value for the liquid branch without displaying any intermediate values. The sharp increase in δ suggests that once rearrangements commenced and (KCl)$_{32}$ melted, the cluster never transformed back into the solidlike phase and subsequently remained in it for any significant amount of time. Hence, we were unable to find any evidence for sustained dynamic coexistence of solidlike and liquidlike forms of (KCl)$_{32}$ in either constant energy or temperature MD simulations. This result is surprising since, as we stated above, the rounding of the transition region in the caloric curve for a finite system is suggestive of a solidlike/liquidlike phase coexistence.

In contrast to (KCl)$_{32}$, for small clusters, both rare gases[1,2,9,13] and alkali halides,[24] $\delta(E)$ displays intermediate values between the solidlike and liquidlike branches, and simulations reveal measurable equilibrium [liquid]/[solid] ratios over ranges of T. From these results it appears that the melting of (KCl)$_{32}$, at least on the ns times scale of our simulations, resembles more a large finite system than the microscopic systems that exhibit a dynamic coexistence between distinct forms for a finite range of temperatures.

The failure of (KCl)$_{32}$ to exhibit any semblance of sustained dynamic phase coexistence is either a manifestation of a sharp dependence of the [liquid]/[solid] equilibrium ratio on T, a very long time scale for passage between the liquidlike and solidlike forms of (KCl)$_{32}$, or a combination of both of these effects. If the absence of dynamic coexistence of solidlike and liquidlike forms of (KCl)$_{32}$ is a consequence of very long passage times, then in extremely long simulations we would expect to observe repeated passages of (KCl)$_{32}$ between its liquidlike state and its solidlike state, consistent with the recent analysis of the full phase diagram of the Ar$_{55}$ cluster by Cheng et al.[64]

Although (KCl)$_{32}$ apparently does not exhibit any dynamic phase coexistence it does show a kind of simultaneous phase coexistence in the form of structures [cf. Fig. 1(d)], both dynamic and quenched, that are simultaneously partly solidlike (ordered) and partly liquidlike (disordered). The liquidlike portions do not wet the solidlike portions therefore we label structures that exhibit this behavior, "nonwetted." We discuss the nonwetted structures in the next section.

B. Nonwetting

In general, phase coexistence occurs when there are two or more observable stable phases for a given complete set of thermodynamic variables. We distinguish two kinds of phase coexistence, dynamic and quasistatic. These terms are best defined in terms of an ensemble of systems exhibiting one of these kinds of phase coexistence and with the two phases being solid and liquid. Consider a large ensemble of systems; the systems may either be microscopic or macroscopic, for now the distinction is not relevant. If at any instant, at fixed temperature and pressure, the ensemble is composed of systems that are each either entirely solid or entirely liquid, then we term this type of coexistence dynamic. We use the expression "dynamic coexistence" because if we employ the ergodic hypothesis and replace the ensemble with a single long-time trajectory, then along this trajectory the system will sometimes be entirely liquid and sometimes entirely solid. A single system then, exhibits a dynamic equilibrium similar to a molecular isomeric equilibrium. Quasistatic coexistence occurs if, at any instant, almost all of the systems of the ensemble exhibit both solid and liquid phases that are in physical contact within each system. We call this type of coexistence "quasistatic" because both phases are observable in one sample system at the same instant of time. Bulk systems exhibit only quasistatic phase coexistence but clusters may exhibit both types of phase coexistence.

If solid and liquid phases are in quasistatic coexistence then the coexistence can be manifested in one of two ways; the liquid melt either may "wet" the solid uniformly or it may not wet the solid. An example of quasistatic coexistence in clusters whose melt wets the solid occurs with Ar$_{147}$, the third Mackay icosohedron, with a complete outer shell of atoms. Both computer simulations and analytical theory[33] have shown that the outer shell of atoms in Ar$_{147}$ melts and becomes liquidlike at temperatures below the homogeneous melting temperature. The entire surface is, averaged over a few tens of vibrations, uniform and liquidlike and thus the liquid surface layer must "wet" the defect-free, inner solidlike core.

The combination of the ionic nature of alkali halides and the density differences of their liquids and solids produces enough repulsive interaction between the interacting solid and liquid surfaces that alkali halide crystals are not wet by the molten salts. In particular, the most common face, the {100} plane, of the crystal is not wet by its melt.[65] Like the bulk alkali halides, (KCl)$_{32}$ also exhibits nonwetting behavior. The demonstration of nonwetting behavior in an alkali halide cluster was first apparent in an earlier study on (NaCl)$_{108}$.[15] Figure 1(d) is an example of a quenched, nonwetted structure. Notice how one part of the cluster is ordered and in the rocksalt structure, while the other portion, disordered and irregular, does not spread to uniformly cover the surface of the crystalline portion. Many quenched structures were viewed on the computer and not one exhibited the liquid portion spread onto the solidlike portions. The nonwetting behavior of (KCl)$_{32}$ is yet another example of phase phenomena that has both microscopic and macroscopic homologues.

In a MD study of the melting of alkali halide micro-crystals composed of 512 ions Amini and co-workers reported that at about 80 K below the freezing temperature the surface ions were found to diffuse and change place with their neighbors.[66] As more energy is put into the system the diffusion propagates into the interior of the microcrystal and the core ions begin to change places with their neighbors. However, Amini and co-workers do not reveal whether the surface melting spreads uniformly over the surface and wets the core ions or if the surface melting nonwets the core.

C. Density of configurational states

We have made several references to the density of configurational states $G(\phi)$ for (KCl)$_{32}$. Clearly, it would be useful if we could calculate it. The density of configurational states, $G(\phi)$, is defined so that $G(\phi)d\phi$ is the total number of inherent structures with equilibrium energy ϕ in the energy range $d\phi$ around ϕ. In $G(\phi)$ we are considering only the density of "configurational" states and are not counting the total density of states which includes, of course, a vibrational contribution. Also, $G(\phi)$ does not reflect the number of permutational isomers, $[(N/2)!]^2$, of each geometrically unique minimum. We present here a method to calculate $G(\phi)$ that only requires easily obtained simulation data for its evaluation. The good degree of quantitative accuracy of this method is demonstrated by comparing a caloric curve derived using our method with a caloric curve based on a constant temperature simulation.

This method is a hybrid of ideas that Stillinger and Weber,[59] Stillinger,[67] and Bixon and Jortner[11] used to calculate partition functions. We begin, like Stillinger, by expressing the total partition function as a double sum over two kinds of microstates; an inner sum over the vibrational states associated with a particular minimum and an outer sum over all the relevant stable minima. Next, as done by Bixon and Jortner, we extract from the outer sum the term representing the vibrational states associated with the ground state configuration. The resultant partition function becomes a sum of two terms: The first term corresponds to the phase space of the ground state configuration and the second term corresponds to the remaining phase space of the excited configurations. In practice, because the distribution of excited minima is essentially continuous we will take the sum over the excited configurations as an integral. Putting these two steps together, we obtain the partition function which, at this stage is as exact for atomic vibrations as the continuum approximation allows:

$$Z_t(\beta) = \frac{e^{-\beta\phi_g}Z_{\text{vib}}(\beta,\phi_g)}{\sigma(0)}$$
$$+ \int_{\phi_l}^{\phi_u} \frac{e^{-\beta\phi}Z_{\text{vib}}(\beta,\phi)G(\phi)}{\sigma(\phi_g)}d\phi, \qquad (3)$$

where ϕ_g is the energy of the ground state, ϕ is the quenched energy of the excited state, $\sigma(\phi)$ is the symmetry number of a minimum with energy ϕ, $Z_{\text{vib}}(\beta,\phi)$ is the vibrational partition function of any minimum with energy

ϕ (we assume there are no exact degeneracies of geometrically inequivalent configurations), ϕ_u is the energy of the least stable configuration, and ϕ_l is the energy of the lowest excited state. From the symmetry point group of the ground state we find $\sigma(\phi_g) = 24$ and as an approximation we set $\sigma(\phi \neq 0) = 1$. There is no $1/[(N/2)!]^2$ term in front of the integral because as we already stated $G(\phi)$ accounts for only the number of geometrically nonequivalent inherent structures.

With this expression for the partition function we can write down the normalized probability, $P(\phi,T)$, that (KCl)$_{32}$ will be found vibrating around an equilibrium configuration with equilibrium energy ϕ, for a given temperature T,

$$P(\phi,T) = \frac{e^{-\beta\phi}Z_{\text{vib}}(\beta,\phi)G(\phi)}{Z_t(\beta)}. \qquad (4)$$

$P(\phi,T)$ is defined here the same as it was above, but for notational consistency we now write $P(\phi,\beta)$ instead of $P(\phi,T)$. If we knew $P(\phi,\beta)$ then we could use Eq. (4) to solve for $G(\phi)$

$$G(\phi) = \frac{P(\phi,\beta)Z_t(\beta)}{e^{-\beta\phi}Z_{\text{vib}}(\beta,\phi)}. \qquad (5)$$

Before we can evaluate $G(\phi)$ we need to calculate $P(\phi,\beta)$, $Z_t(\beta)$, and $Z_{\text{vib}}(\beta,\phi)$. $Z_t(\beta)$ is just a number that acts as a normalization constant for $P(\phi,\beta)$ and it will be left as a free parameter.

To calculate $P(\phi,\beta)$ we used a sampling method somewhat like one introduced recently by Labastie and Whetten for Monte Carlo simulations.[68] We performed several constant temperature simulations at the same value of β, call it β'. The simulation can be done either by Monte Carlo or MD procedure; for this study we used MD. During each constant temperature trajectory we regularly quenched the cluster to determine the inherent minima within which the cluster was vibrating. This process was repeated for several trajectories at β' until about 1000 quenched energies were accumulated. Several short trajectories (i.e., trajectories based on different initial conditions) were used instead of one long one in order to minimize any peculiar effects the initial conditions might have on the results. The accumulated quenched energies were binned and smoothed to obtain a numerical representation of the unnormalized $P(\phi,\beta')$.

To be of most practical use we should have an analytical representation for $P(\phi,\beta')$. To construct this, we fit the numeric data to a continuous function using a nonlinear least-squares fit. The least-squares fit of $P(\phi,\beta')$ is integrated and then normalized. This process worked well; the numeric and analytic representations for $P(\phi,\beta')$ are shown in Fig. 8. We chose to evaluate $P(\phi,\beta')$ at $T=805$ K because it was high enough above the melting temperature to provide a wide distribution of ϕ values but not too high to obscure any interesting details. The analytic representation we chose for $P(\phi,\beta')$ was a sum of two Gaussians
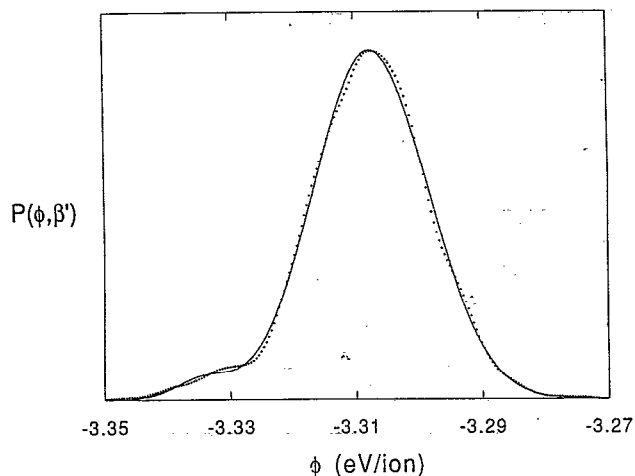
FIG. 8. Probability distribution function $P(\phi,\beta')$, $\beta' = (k_B 805)^{-1}$; points are the numeric data from simulations and the solid line is a nonlinear least-squares fit of the numeric data using Eq. (6). ϕ represents the quenched energy of a stable structure of (KCl)$_{32}$. The parameters of the two-Gaussian fit are listed in Table II.

$$P(\phi,\beta') = \frac{A_1}{\sqrt{2\pi}\sigma_1} \exp\left[\frac{-(\phi - m_1)^2}{2\sigma_1^2}\right]$$
$$+ \frac{A_2}{\sqrt{2\pi}\sigma_2} \exp\left[\frac{-(\phi - m_2)^2}{2\sigma_2^2}\right]. \qquad (6)$$

See Table II for the values of the Gaussian parameters.

Next we need to calculate $Z_{\text{vib}}(\beta,\phi_g)$ and $Z_{\text{vib}}(\beta,\phi)$. For $Z_{\text{vib}}(\beta,\phi_g)$ we use a classical $3N-6$ harmonic oscillator vibrational partition function multiplied by a temperature dependent exponential function that accounts for anharmonic effects

$$Z_{\text{vib}}(\beta,\phi_g) = \exp\left(\frac{\gamma_g}{\beta}\right) \prod_{j=1}^{3N-6} [h\nu_j(\phi_g)\beta]^{-1}. \qquad (7)$$

$\nu_j(\phi_g)$ are the normal mode frequencies of the ground state and γ_g is the anharmonic constant for the ground state; γ_g was determined by fitting the theoretical caloric curve derived from $Z_{\text{vib}}(\beta,\phi_g)$ to numerical data from simulation, i.e., the points of the caloric curve below the onset of melting. For the vibrational partition functions associated with excited minima, we do basically the same thing except that we use a different anharmonic constant

$$Z_{\text{vib}}(\beta,\phi) = \exp\left(\frac{\gamma_e}{\beta}\right) \prod_{j=1}^{3N-6} [h\nu_j(\phi)\beta]^{-1}, \qquad (8)$$

TABLE II. Values of the parameters used to calculate $G(\phi)$ in Eq. (13).

A_1	0.9712		γ_g	1.875×10^5 ion/eV	
m_1	0.0629	eV/ion	γ_e	2.7×10^4 ion/eV	
σ_1	9.0853×10^{-3} eV/ion		a	$-1.12\,739$	
A_2	0.0288		b	364.986 ion/eV	
m_2	0.0362	eV/ion	c	-715.631 ion/eV^2	
σ_2	4.4535×10^{-3} eV/ion		d	9456.92 ion/eV^3	

where γ_e is the anharmonic constant for the excited minima and $\nu_j(\phi)$ are the normal mode vibrational frequencies for minima with energy ϕ. The constant γ_e is determined essentially the same way as γ_g, but in this case we use numerical data from simulations of liquidlike (KCl)$_{32}$, i.e., from the points of the caloric curve above the melting range. Only one γ_e was used for all the excited minima. However, if a more accurate description is desired then γ_e could be expressed as a function of ϕ, $\gamma_e(\phi)$. Since it is not possible for us to evaluate the frequencies $\nu_j(\phi)$ for each individual excited minimum we need some approximate expression that accounts for the softening of the phonon spectrum as ϕ increases. We follow an approach similar to that of Stillinger and Weber[56] and express $Z_{\text{vib}}(\beta,\phi)$ as a product of $Z_{\text{vib}}(\beta,\phi_g)$ and a ϕ-dependent function

$$\prod_{j=1}^{3N-6} [h\nu_j(\phi)\beta]^{-1} = \exp[q(\phi)] \prod_{j=1}^{3N-6} [h\nu_j(\phi_g)\beta]^{-1}. \qquad (9)$$

Solving for $q(\phi)$ and approximating it by a cubic polynomial we get

$$q = a + b\phi + c\phi^2 + d\phi^3$$
$$= \sum_{j=1}^{3N-6} \ln \nu_j(\phi_g) - \sum_{j=1}^{3N-6} \ln \nu_j(\phi). \qquad (10)$$

The coefficients of the polynomial can be found by plotting the right side of Eq. (10), for many different minima, against ϕ. The simulation data needed to do this can be obtained from the same simulations performed to find $P(\phi,\beta')$. See Table II for the values of the polynomial coefficients.

We now rewrite Eq. (3) by replacing $G(\phi)$ with Eq. (5) evaluated at $\beta = \beta'$

$$Z_t(\beta) = \frac{e^{-\beta\phi_g} Z_{\text{vib}}(\beta,\phi_g)}{24}$$
$$+ \int_{\phi_l}^{\phi_u} \frac{e^{-\beta\phi} Z_{\text{vib}}(\beta,\phi) P(\phi,\beta') Z_t(\beta')}{e^{-\beta'\phi} Z_{\text{vib}}(\beta',\phi)} d\phi. \qquad (11)$$

This equation for $Z_t(\beta)$ is used in the canonical ensemble equation

$$E = k_B T^2 \frac{\partial \ln [Z_t(\beta)]}{\partial \beta} \qquad (12)$$

to provide an expression, parametrized by $Z_t(\beta')$ and γ_e, for the constant temperature caloric curve that we can compare to simulation data. [At this point γ_e and $Z_t(\beta')$ are still unknown.] The integral in the expression for $Z_t(\beta)$ can easily be done numerically with the error function. Over the important range of values of β the integral is robust to changes in the integration limits. That is, the lower limit could be made much smaller and the upper limit much higher without noticeable changes in the value of the integral. This means the approximate values of ϕ_l

and ϕ_u obtained from simulation results did not introduce any significant error. This is true because at the important values of β, not too high and not too low, the high-lying and low-lying minima are visited very infrequently by the cluster and so $P(\phi,\beta)$ is negligible at these extreme values of ϕ.

It was a simple task to find the values of $Z_t(\beta')$ and γ_e because their effects are independent of each other, adjusting the value one parameter did not alter the effects of the other parameter. The magnitude of γ_e was determined by

matching the liquidlike portion of the model curve with the simulation caloric curve. $Z_t(\beta')$ is just a normalization constant which fixes the melting temperature and was adjusted to match the melting region of the model caloric curve with the simulation data. The simulation and model caloric curves are shown in Fig. 9. The goodness of fit tells us that the analytic representation for $P(\phi,\beta')$ is quantitatively fairly accurate.

The final step to obtain $G(\phi)$ is to express Eq. (5) in terms of all the known quantities

$$G(\phi) = \frac{\left\{\dfrac{A_1}{\sqrt{2\pi}\sigma_1}\exp\left[\dfrac{-(\phi-m_1)^2}{2\sigma_1^2}\right] + \dfrac{A_2}{\sqrt{2\pi}\sigma_2}\exp\left[\dfrac{-(\phi-m_2)^2}{2\sigma_2^2}\right]\right\}Z_t(\beta')}{\exp(-\beta'\phi)\exp\left(\dfrac{\gamma_e}{\beta'}\right)\exp[q(\phi)]Z_{\text{vib}}(\beta',\phi_g)}. \tag{13}$$

The natural log of $G(\phi)$ and its derivative with respect to ϕ are shown in Fig. 10. There are a few important points concerning the two curves in Fig. 10 that should be discussed. First, the calculated $\ln[G(\phi)]$ is negative for very low values of ϕ which is of course unphysical. This error can be due to the values of $Z_t(\beta'),\gamma_e$, or from the fitting function $q(\phi)$, but it is most likely a result of fitting the numeric data of $P(\phi,\beta')$ at very low values of ϕ to a sum of two Gaussians. This error is not significant because the values of ϕ for which $G(\phi)$ is negative are unimportant thermodynamically. Furthermore, the approximation that $G(\phi)$ is continuous probably fails for these extreme low values of ϕ.

Labastie and Whetten[68] have employed a similar method to compute the total density of states, in contrast to the density of configurational states calculated here. Their method was similar in that they also computed a function $P(\phi,\beta)$, but in their case ϕ represented the instantaneous configurational energy of the cluster. Their recipe was to use Monte Carlo simulations to compute $P(\phi,\beta)$ for several different nearby values of β. This allowed the ratio of the partition functions for the different values of the β, and ultimately the density of total-energy states, to be computed. If necessary this method could be applied here as well. In the future this should be done in order to compare the two methods. If the agreement between the results of the two methods is good then the two methods would mutually validate each other.

It has been postulated that the total number of nonequivalent equilibrium structures of a cluster, Ω_t, increases exponentially with the number of particles N

$$\Omega_t = \int_{\phi_l}^{\phi_u} G(\phi)d\phi = e^{\alpha N} \tag{14}$$

where the exponential constant is of order unity.[51,69] The value of α depends on the type of cluster but for large clusters it should be independent of size. If we use a maximum term approximation for Ω_t, i.e., $\Omega_t = G(\phi_u)$, then

using this data for (KCl)$_{32}$ we find that for KCl clusters $\alpha \approx 0.66$. If we assume that KCl clusters in general have a $G(\phi)$ qualitatively similar to the one for (KCl)$_{32}$ then we can obtain $G(\phi)$ for other KCl clusters simply by using our calculated value of α to calculated Ω_t and then use Ω_t to renormalize $G(\phi)$ to the correct magnitude for the new cluster size. Obviously, this is only true for large KCl clusters for which a continuous form can be used for $G(\phi)$.

From the derivative of $\ln[G(\phi)]$ with respect to ϕ shown in Fig. 10(b) we see that there is a ϕ at which the slope becomes negative. This ϕ indicates the energy at which equilibrium structures with evaporated particles or just unrealistically noncompact structures begin to dominate the potential energy surface landscape and thus should correspond with the value of ϕ_u chosen on the basis of simulation results. The fact that the two do agree displays a kind of self-consistency that is indirect demonstration of the validity of this approach.
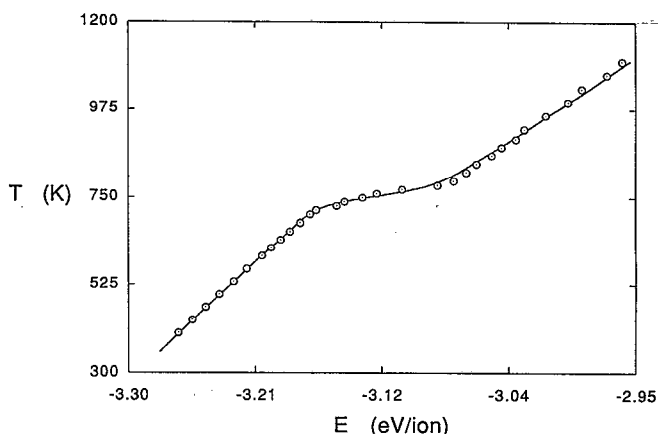
FIG. 9. Constant temperature caloric curve for (KCl)$_{32}$; points are simulation data and the solid line is the theoretical fit using Eq. (11) in Eq. (12).
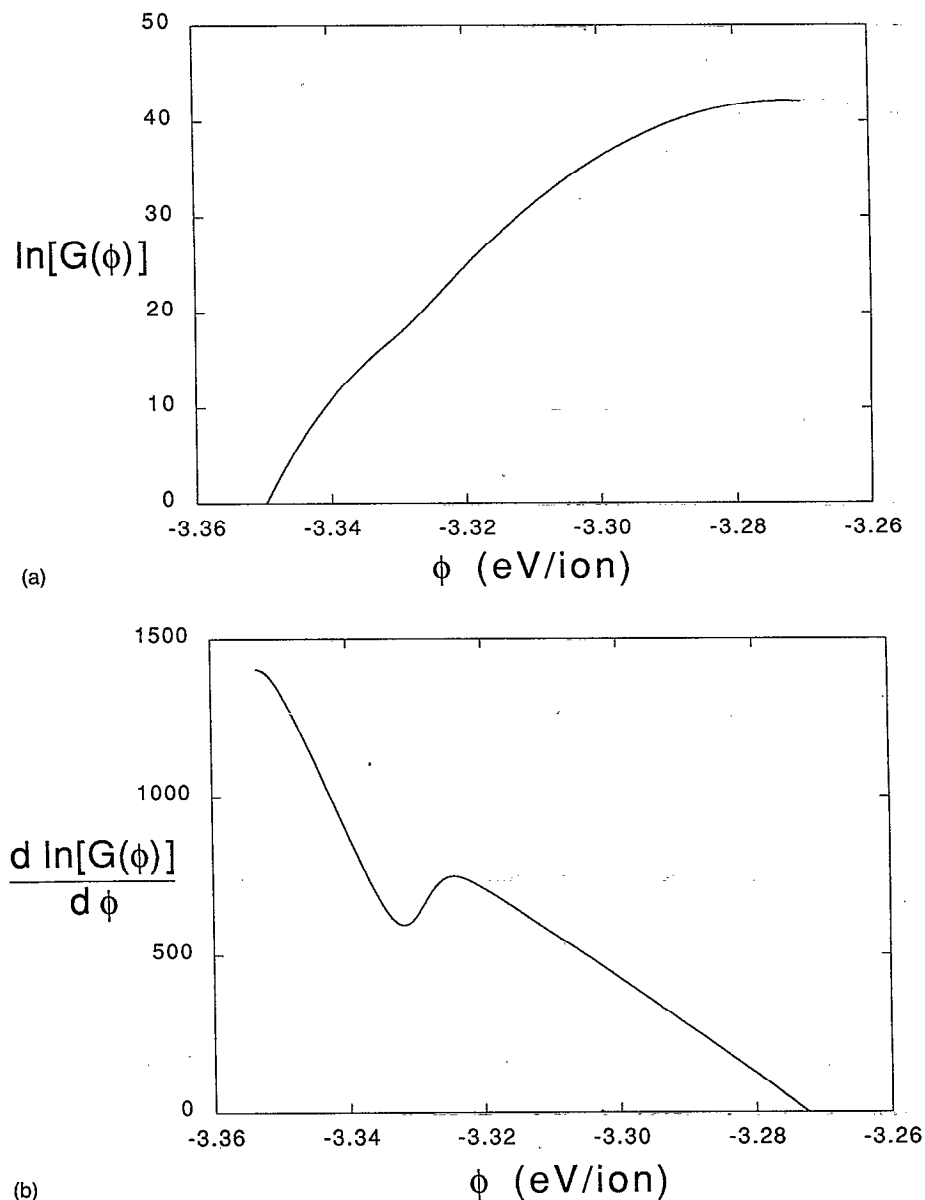
FIG. 10. Density of configurational states: (a) log of configurational density of states $\ln[G(\phi)]$ (b) ϕ-derivative of the function shown in (a). ϕ represents the quenched energy of a stable structure of $(KCl)_{32}$.

IV. INTERPRETATIONS AND CONCLUDING REMARKS

From constant energy simulations we found that $(KCl)_{32}$ exhibits a solidlike low temperature phase and a liquidlike high temperature phase. $(KCl)_{32}$ transforms between these two phases in a very small energy interval. That is, once the energy of $(KCl)_{32}$ is high enough, the cluster passes out of its microcrystal solidlike state and rarely finds its way back to it or any of the other low-lying, crystalline minima, and if it does, its stay is only transitory. This conclusion is supported by the fact that we found no evidence of a dynamic coexistence, at least on the nsec time scale of our MD simulations, between solid and liquid $(KCl)_{32}$. This is a salient distinction with the small KCl clusters, which exhibit a dynamic coexistence between low-potential energy (global minimum) and high-potential en-

ergy forms that is observable on the time scale of MD simulations, for a measurable range of energies.[24]

The liquidlike phase of $(KCl)_{32}$, the second KCl magic number cluster, is more fluid than the stiff liquidlike state of $(KCl)_4$, the first KCl magic number cluster. The liquidlike state of $(KCl)_4$ is characterized by highly collective interwell motions with particle interchanges occurring through a multistep process. The interwell motions of $(KCl)_{32}$ are less collective and are more facile as evidenced by its large diffusion constant; this is also apparent in animations of the MD on the computer. In these respects the liquidlike phase of $(KCl)_{32}$ is more like the bulk liquid phase than the liquidlike state of small KCl clusters. Hence, it is without question perfectly appropriate to speak about the "phases" of $(KCl)_{32}$ in the sense that we do for

bulk systems. (KCl)$_{32}$ is a prime example of how a microscopic system can exhibit distinct phases that are unambiguously identifiable with bulk phases.

We found that (KCl)$_{32}$ has quenched structures that are a combination of regular, ordered, and irregular, disordered parts. Dynamically we associate the regular part with the solidlike state and the disordered part with the liquidlike state, or with its frozen-out counterpart. Thus, these structures define a type of simultaneous phase coexistence that we term nonwetting, the solid is "not wetted" by the liquid. Applying the term "phase coexistence" to these nonwetted structures is loose use of terms since we have not rigorously demonstrated that the nonwetted structures define a physically distinct, stable phase of (KCl)$_{32}$. That is, we did not resolve the nonwetted behavior from the general liquidlike behavior of (KCl)$_{32}$ in any physically attainable way, only by unrealistic mathematical quenching procedures. We nevertheless employ this term to permit comparisons with the behavior of the surface melted state of some rare gas clusters, where the melted surface layer "wets" the solid inner core. This melted surface state is a stable antecedent phase of the homogeneously melted cluster.[33] At high temperatures the stability of nonwetted (KCl)$_{32}$ structures gives way to completely disordered, amorphous structures. These structures are unusual in their conspicuous lack of order. We use this present mention of amorphous (KCl)$_{32}$ to pose the question concerning the possible existence of a microamorphous phase that is the small-system analog of the bulk glass phase. We have investigated this question using (KCl)$_{32}$ as the model system and the results are in the following paper.[70]

We outlined a method by which one can calculate the static configurational density of states $G(\phi)$. This same method also allows one to calculate the total canonical partition function from which the free energy is calculable. The quantitative accuracy of the method was shown by comparing a constant temperature MD caloric curve with the one derived from our model partition function.

Stillinger[67] proposed a simple form for $G(\phi)$ based on a combinatorics approach to a system of dilute noninteracting vacancy defects

$$G(\phi) = \exp[\epsilon_v \phi \ln \phi + O(\phi)], \qquad (15)$$

where ϵ_v is the enthalpy of creating a defect and ϕ is the energy difference between the packing energy of the ground state and the defected minimum. Stilliger comments in relation to this expression for $G(\phi)$ that "inclusion of other types of point defects, and of a finite number of defect configurations at any location within the crystalline matrix would not alter the basic functional form of Eq. (15)." With appropriate choices for ϵ_v and ϕ the functional form shown in Eq. (15) fits well the $G(\phi)$ that we calculated for (KCl)$_{32}$. This implies that the qualitative form of $G(\phi)$ that we calculated for (KCl)$_{32}$ is probably generally applicable to large clusters and possibly to bulk systems. In other words, maybe there is a sort of law of corresponding states for $G(\phi)$. However, one major difference between Eq. (15) and the density of configurational
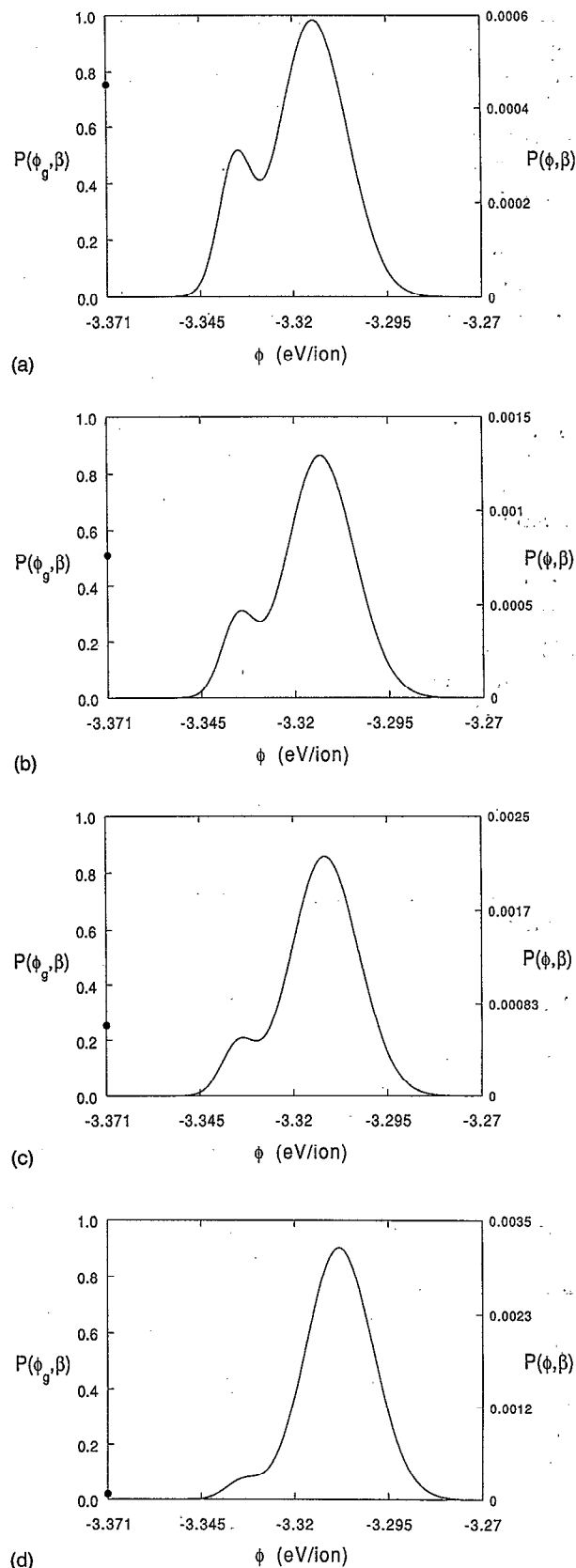
FIG. 11. Fraction of (KCl)$_{32}$ clusters, $P(\phi,\beta)$, occupying a basin with minimum energy ϕ for a given temperature. In each curve the left axis corresponds to $P(\phi_g,\beta)$ and the solid circle on the left axis marks the $P(\phi_g,\beta)$ value. The right axis corresponds to the distribution of $P(\phi,\beta)$ values for excited state configurations: (a) $T=737.5$ K, (b) $T=751$ K, (c) $T=765$ K, and (d) $T=800$ K.

states of (KCl)$_{32}$ that we calculated is the slope of $G(\phi)$ as ϕ approaches zero. The slope of Eq. (15) diverges as ϕ approaches zero whereas the slope of the $G(\phi)$ that we calculated stays finite [Fig. 10(b)]. If our evaluation of $G(\phi)$ is at least qualitatively correct insofar as the slope approaches a finite limiting value as ϕ approaches zero, then this is a major distinction between large clusters and bulk—a diverging slope of $G(\phi)$ may be found only for bulk systems. The limit of this slope, as the size of the system increases, can be used to monitor the approach from small system behavior to bulk behavior.

In Sec. III we discussed the phase behavior of (KCl)$_{32}$ as investigated by constant energy MD simulations. Here we use our model partition function to analyze the phase behavior of (KCl)$_{32}$. The partition function we formulated for (KCl)$_{32}$ allows us to compute the fraction or probability, $P(\phi,\beta)$, of (KCl)$_{32}$ clusters occupying a potential surface basin with minimum energy ϕ at a given β,

$$P(\phi,\beta) = \frac{Z_\phi(\beta)}{Z_t(\beta)} . \qquad (16)$$

$Z_\phi(\beta)$ is the contribution to the total partition function $Z_t(\beta)$ [Eq. (11)] from basins with energies of minima in the range $\phi \pm \delta\phi$,

$$Z_\phi(\beta) = \frac{e^{-\beta\phi_g}Z_{\text{vib}}(\beta,\phi_g)}{24} \bigg|_{\phi=\phi_g} \qquad (17a)$$

and

$$Z_\phi(\beta) = \frac{e^{-\beta\phi}Z_{\text{vib}}(\beta,\phi)P(\phi,\beta')Z_t(\beta')}{e^{-\beta'\phi}Z_{\text{vib}}(\beta'\phi)} d\phi \bigg|_{\phi>\phi_g} . \qquad (17b)$$

In Fig. 11 we show the plots of Eq. (16) for several temperatures.

At low temperatures (not shown) $P(\phi_g,\beta) = 1$, where ϕ_g is the value of ϕ for the global minimum, rocksalt basin. As the temperature is increased to the lower end of the transition region [Fig. 11(a)] $P(\phi_g,\beta)$ decreases below unity and a significant distribution of $P(\phi,\beta)$ develops for the excited-state basins ($\phi > \phi_g$). Thus for this temperature $P(\phi,\beta)$ can be decomposed into two main parts; a delta-function distribution at ϕ_g (≈ 0.75) and a second distribution (≈ 0.25) over all the higher values of ϕ. It is significant that the distribution of $P(\phi,\beta)$ values over the excited-state basins has a peak shape and is not monotonically decreasing with ϕ. Upon further increase of T, $P(\phi_g,\beta)$ decreases until it is equal to the area under the distribution of $P(\phi,\beta)$ for the excited-state basins [Fig. 11(b)]. This temperature defines the melting point of (KCl)$_{32}$. As T is increased above the melting temperature, $P(\phi_g,\beta)$ decreases rapidly and, equally as fast, the area under the distribution of $P(\phi,\beta)$ over the excited-state basins approaches unity. Eventually $P(\phi_g,\beta)$ approaches a negligible value and $P(\phi,\beta)$ is significant only for the upper values of ϕ.

Based on the MD simulations results we interpret each part of $P(\phi,\beta)$ ($\phi=\phi_g$ and $\phi>\phi_g$) as representing a physically distinct form of (KCl)$_{32}$. Specifically, we identify the
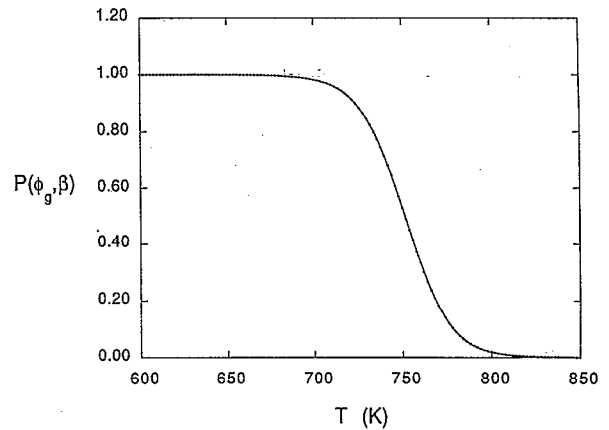
FIG. 12. $P(\phi_g,\beta)$ as a function of temperature.

fraction $P(\phi_g,\beta)$ with the fraction of solidlike clusters in an ensemble of (KCl)$_{32}$ clusters. Likewise, for all temperatures within and above the transition region we identify the high-ϕ distribution of $P(\phi,\beta)$ with the liquidlike state of (KCl)$_{32}$. Although at first glance these findings appear so, they are in fact not contradictory to the simulation results in which we found no evidence for a sustained dynamic coexistence of solidlike and liquidlike forms of (KCl)$_{32}$. The statistical approach used here overcomes the time scale limitations and dynamical effects associated with MD simulations that prohibit observation of the solidlike/liquidlike dynamic phase coexistence. More importantly these findings suggest that the inability to observe, in MD simulations, a dynamic coexistence between solidlike and liquidlike forms of (KCl)$_{32}$ is most likely due to very long passage times between the two phases. This specific finding will be discussed in more detail elsewhere. Finally, this is yet another example of the interplay of dynamics and thermodynamics in clusters.[71]

Note, that the distribution of $P(\phi,\beta)$ over the excited-state basins actually has two peaks and that we might consider the total $P(\phi,\beta)$ distribution to have three significant parts. The appearance of two high-ϕ peaks could be an artifact of fitting the numerical representation of $P(\phi,\beta')$ to a sum of two Gaussians. However, we ignore the existence of the second minor peak since this does not alter our basic conclusions. These calculations can be repeated using the Labastie and Whetten[68] histogram method to verify if the splitting of the high-ϕ distribution of $P(\phi,\beta)$ is real or just an artifact of this specific method.

We computed $P(\phi_g,\beta)$ as a function of temperature to show how rapidly it decreases from unity down to zero and the result is shown in Fig. 12. The S-shape region of this curve defines the range of temperatures within which an ensemble of (KCl)$_{32}$ clusters consists of significant fractions of both solidlike and liquidlike clusters. Hence, we conclude that for a range of temperatures (KCl)$_{32}$ has two stable forms; a solidlike form identified with ϕ_g (Ref. 72) and a liquidlike form identified with a temperature-dependent distribution of excited-state basins. The main significance of this result is that it directly relates the sol-

idlike and liquidlike forms of a cluster with specific basins of the potential energy surface—a dominant theme in our studies of the phase behavior of clusters. Lastly, since we arrived at this conclusion from a statistical approach it stands up to criticisms concerning possible nonequilibrium effects associated with MD simulations.

ACKNOWLEDGMENTS

[1] J. Jellinek, T. Beck, and R. S. Berry, J. Phys. Chem. **84**, 2783 (1986).

[2] F. G. Amar and R. S. Berry, J. Chem. Phys. **85**, 5943 (1986).

[3] J. D. Honeycutt and H. C. Anderson, J. Phys. Chem. **91**, 4950 (1987).

[4] R. S. Berry, T. L. Beck, H. L. Davis, and J. Jellinek, in *Evolution of Size Effects in Chemical Dynamics*, Part 2, edited by I. Prigogine and S. A. Rice, Adv. Chem. Phys. **70**, Part 2, 75 (1988).

[5] R. S. Berry, P. Braier, R. J. Hinde, and H. P. Cheng, Isr. J. Chem. **30**, 39 (1990).

[6] J. E. Adams and R. M. Stratt, J. Chem. Phys. **93**, 1332 (1990).

[7] F. H. Stillinger and D. K. Stillinger, J. Chem. Phys. **93**, 6013 (1990).

[8] P. A. Braier, R. S. Berry, and D. J. Wales, J. Chem. Phys. **93**, 8745 (1990).

[9] T. L. Beck, J. Jellinek, and R. S. Berry, J. Chem. Phys. **87**, 545 (1987).

[10] T. L. Beck and R. S. Berry, J. Chem. Phys. **88**, 3910 (1988).

[11] M. Bixon and J. Jortner, J. Chem. Phys. **91**, 1631 (1989).

[12] R. S. Berry, Z. Phys. D **12**, 161 (1989).

[13] D. J. Wales and R. S. Berry, J. Chem. Phys. **92**, 4283 (1990).

[14] D. O. Welch, O. W. Lazareth, G. J. Dienes, and R. D. Hatcher, J. Phys. Chem. **64**, 835 (1976).

[15] D. O. Welch, O. W. Lazareth, G. J. Dienes, and R. D. Hatcher, J. Chem. Phys. **68**, 2159 (1978).

[16] T. P. Martin, J. Chem. Phys. **67**, 5207 (1977).

[17] T. P. Martin, J. Chem. Phys. **69**, 2036 (1978).

[18] T. P. Martin, J. Chem. Phys. **72**, 3506 (1980).

[19] T. P. Martin, Phys. Rep. **95**, 169 (1983).

[20] J. Diefenback and T. P. Martin, J. Chem. Phys. **83**, 4585 (1985).

[21] J. Luo, U. Landman, J. Jortner, in *Physics and Chemistry of Small Clusters*, edited by P. Jena, B. K. Rao, and S. Khanna, NATO ASI Series B (Plenum, New York, 1987), Vol. 158, p. 155.

[22] A. Heidenreich, I. Schek, D. Scharf, and J. Jortner, Z. Phys. D **20**, 227 (1991).

[23] A. Heidenreich, I. Schek, D. Scharf, and J. Jortner, J. Phys. Chem. (submitted).

[24] J. Rose and R. S. Berry, J. Chem. Phys. **96**, 517 (1992).

[25] N. G. Phillips, C. W. S. Cononver, and L. A. Bloomfield, J. Chem. Phys. **94**, 4980 (1991).

[26] J. E. Adams and R. M. Stratt, J. Chem. Phys. **93**, 1358 (1990).

[27] L. F. Fried and S. Mukamel, Phys. Rev. Lett. **66**, 2340 (1991).

[28] N. H. Kaukonen, U. Landman, and C. L. Cleveland, J. Chem. Phys. **95**, 4997 (1991).

[29] R. N. Barnett, U. Landman, A. Nitzan, and G. Rajagopal, J. Chem. Phys. **94**, 608 (1991).

[30] J.-Y. Yi, D. J. Oh, and J. Bernholc, Phys. Rev. Lett. **67**, 1594 (1991).

[31] S. Sawada and S. Sugano, Z. Phys. D **12**, 189 (1989).

[32] S. Sawada and S. Sugano, Z. Phys. D **14**, 247 (1989).

[33] H. P. Cheng and R. S. Berry, Phys. Rev. A **45**, 7969 (1992).

[34] R. S. Berry, H. P. Cheng, and J. Rose, High Temp. Sci. **27**, 61 (1990).

[35] L. S. Bartell, E. J. Valente, and T. S. Dibble, J. Phys. Chem. **94**, 1452 (1990).

[36] L. S. Bartell, L. Harsanyi, T. S. Dibble, and P. J. Lennon, J. Phys. Chem. **94**, 6009 (1990).

[37] L. S. Bartell, F. J. Dulles, and B. Chuko, J. Phys. Chem. **95**, 6481 (1991).

[38] T. S. Dibble and L. S. Bartell, J. Phys. Chem. **96**, 2317 (1992).

[39] T. P. MArtin, T. Bergmann, and B. Wasserman, in *Microclusters, Proceedings of the First NEC Symposium*, edited by S. Sugano, Y. Nishina, and S. Ohnishi, Hakone and Kawasaki, Japan, October 1986 (Springer, Berlin, 1987).

[40] Proceedings of the Fifth International Meeting on Small Particles and Inorganic Clusters, in Z. Phys. D **19**, Nos. 1–4 (1991) and Z. Phys. D **20**, Nos. 1–4 (1991).

[41] Proceedings of the Faraday Symposium 25 on Large Gas-Phase Clusters, in Royal Soc. Chem. Faraday Trans. **86**, No. 13 (1990).

[42] B. I. Dunlap, J. Chem. Phys. **84**, 5611 (1986).

[43] M. P. Allen and D. J. Tildesley, *Computer Simulation of Liquids* (Clarendon, London, 1987).

[44] D. W. Hermann, *Computer Simulation Methods in Theoretical Physics* (Springer, Berlin, 1986), Chap. 3.

[45] H. L. Friedman, *A Course in Statistical Mechanics* (Prentice-Hall, Englewood Cliffs, 1985), Chap. 5.

[46] S. Nosé, J. Chem. Phys. **81**, 511 (1983).

[47] S. Nosé, Mol. Phys. **52**, 255 (1984).

[48] C. W. Gear, *Numerical Initial Value Problems in Ordinary Differential Equations* (Prentice-Hall, Englewood Cliffs, 1971).

[49] H. L. Davis, J. Jellinek, and R. S. Berry, J. Chem. Phys. **86**, 6456 (1987).

[50] F. H. Stillinger and T. A. Weber, Phys. Rev. A **25**, 978 (1982).

[51] F. H. Stillinger and T. A. Weber, Phys. Rev. A **28**, 2408 (1983).

[52] W. H. Press, B. P. Flannery, S. A. Teukolsky, and W. T. Vetterling, *Numerical Recipes* (Cambridge University, Cambridge, 1986), Chap. 10.

[53] M. P. Tosi and F. G. Fumi, J. Phys. Chem. Solids **25**, 45 (1964).

[54] E. S. Rittner, J. Chem. Phys. **19**, 1030 (1951).

[55] M. Karplus and P. N. Porter, *Atoms and Molecules: An Introduction for Students of Physical Chemistry* (Benjamin/Cummings, Reading, 1970), Chap. 5.

[56] R. S. Berry and D. J. Wales, Phys. Rev. Lett. **63**, 1156 (1989).

[57] D. J. Wales and R. S. Berry, J. Chem. Phys. **92**, 4473 (1990).

[58] D. J. Wales, Chem. Phys. Lett. **166**, 419 (1990).

[59] F. H. Stillinger and T. A. Weber, J. Chem. Phys. **81**, 5095 (1984).

[60] T. Hill, *Thermodynamics of Small Systems* (Benjamin, New York, pt. I, 1963, pt. II, 1964).

[61] I. Z. Fisher, *Statistical Theory of Liquids* (University of Chicago, Chicago, 1966).

[62] I. Gilvarry, Phys. Rev. **103**, 1700 (1956).

[63] J. O'M. Bockris, S. R. Richards, and L. Nanis, J. Phys. Chem. **69**, 1627 (1965).

[64] H.-P. Cheng, X. Li, R. L. Whetten, and R. S. Berry, Phys. Rev. A **46**, 791 (1992).

[65] G. Grange, R. Landers, and B. Mutaftschiev, Surf. Sci. **54**, 445 (1976).

[66] M. Amini, D. Fincham, and R. W. Hockney, J. Phys. C **12**, 4707 (1979).

[67] F. H. Stillinger, J. Chem. Phys. **88**, 7818 (1988).

[68] P. Labastie and R. L. Whetten, Phys. Rev. Lett. **65**, 1567 (1990).

[69] M. R. Hoare, Adv. Chem. Phys. **40**, 49 (1979).

[70] J. P. Rose and R. S. Berry, J. Chem. Phys. **98**, 3262 (1993) (following paper).

[71] R. S. Berry, Z. Phys. D **12**, 161 (1989).

[72] To be exact the solidlike state of (KCl)$_{32}$ should be identified with not only the global minimum basin, but also the very low-lying, crystal-like basins. However, identifying the solidlike state of (KCl)$_{32}$ with only the global minimum, rocksalt basin is an excellent approximation since as can be seen from Fig. 11 $P(\phi,\beta)$ is negligible for the values of ϕ associated with the deep, crystal-like basins.